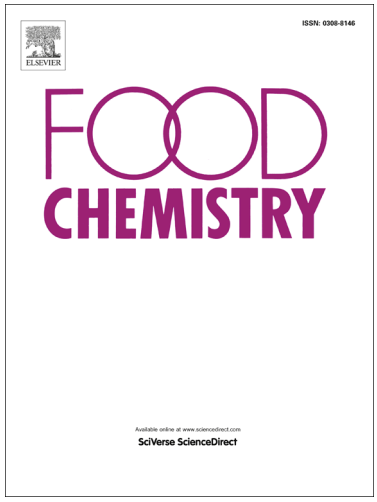

Insights into the multi-scale structure and digestibility of heat-moisture treated rice starch

Hongwei Wang, Yufan Liu, Ling Chen, Xiaoxi Li, Jun Wang, Fengwei Xie

PII: S0308-8146(17)31470-X
DOI: http://dx.doi.org/10.1016/j.foodchem.2017.09.014
Reference: FOCH 21683

To appear in: *Food Chemistry*

Received Date: 17 March 2017
Revised Date: 10 August 2017
Accepted Date: 4 September 2017

Please cite this article as: Wang, H., Liu, Y., Chen, L., Li, X., Wang, J., Xie, F., Insights into the multi-scale structure and digestibility of heat-moisture treated rice starch, *Food Chemistry* (2017), doi: http://dx.doi.org/10.1016/j.foodchem.2017.09.014

Insights into the multi-scale structure and digestibility of heat-moisture treated rice starch

Hongwei Wang[a], Yufan Liu[a], Ling Chen[a,*], Xiaoxi Li[a,*], Jun Wang[b], Fengwei Xie[c]

[a] *Ministry of Education Engineering Research Center of Starch & Protein Processing, Guangdong Province Key Laboratory for Green Processing of Natural Products and Product Safety, College of Light Industry and Food Sciences, South China University of Technology, Guangzhou 510640, China*

[b] *CREPEC, Department of Chemical Engineering, École Polytechnique de Montréal, Montréal, Québec H3T 1J4, Canada*

[c] *School of Chemical Engineering, The University of Queensland, Brisbane, Qld 4072, Australia*

[*] Corresponding authors. Tel.: +86 20 87113252; fax: +86 20 87113252. *Email addresses*: felchen@scut.edu.cn (L. Chen), xxlee@scut.edu.cn (X. Li)

Abstract: The digestibility and structural changes of rice starch induced by heat-moisture treatment (HMT) were investigated, and the relationships among the moisture content–starch structure–starch digestibility were revealed. HMT could simultaneously disorder and reassemble the rice starch molecules across multi-scale lengths and convert some fractions of rapidly-digestible starch (RDS) into slowly-digestible starch (SDS) and resistant starch (RS). In particular, the HMT rice starch with less than 30% moisture content showed a higher SDS + RS content (25.0%). During HMT, SDS and RS were preferably formed by the degraded starch molecules with M_w between 4×10^5 and 4×10^6 g/mol, single helices and amylose-lipids complexes that were formed by degraded starch chains with higher thermal stability and crystalline lamellae with greater thicknesses. Thus, our research suggests a potential approach using HMT to control the digestion of starch products with desired digestibility.

Keywords: starch; heat moisture treatment; *in vitro* digestibility; structural changes

1. Introduction

Rice is the most important cereal crop and the staple food in Asia. However, compared with other starch foods, rice is commonly known as food with a higher glycemic index (GI), ranged from 54 to 121 (Edes & Shah, 1998; Hu, Zhao, Duan, Linlin, & Wu, 2004). The consumption of large amounts of high-GI food may lead to obesity, diabetes, and cardiovascular disorders (Shu, Jia, Ye, Li, & Wu, 2009; Yang, Shu, Zhang, Wang, Zhao, Ma, et al., 2006). Thus, rice with a lower GI should be helpful for avoiding the diet-related diseases.

Starch is the major component (*ca*. 90%) of rice and an important part of human nutrition (Zhou, Robards, Helliwell, & Blanchard, 2002). According to the rate and extent of starch digestion *in vitro*, starch is classified into three major fractions: rapidly-digestible starch (RDS), slowly-digestible starch (SDS) and resistant starch (RS) (Englyst, Vinoy, Englyst, & Lang, 2007). The rate of starch digestion directly relates to the glycemic and insulin responses, and a higher amount of RDS in food leads to a lower GI (Englyst, et al., 2007). On the contrary, SDS and RS may result in slower glucose release and lower glycemic response, suppressing the occurrence of those metabolic diseases (Zhang, Li, Chen, & Situ, 2016). Thus, it is promising to modulate the starch digestibility for the design of low-GI foods with health benefits.

Recently, various approaches (*e.g.*, chemical, physical, genetic, and multiple modifications) have been explored to produce high amounts of SDS and/or RS (Lee & Moon, 2015; Miao, Zhang, Mu, & Jiang, 2010; Shin, Lee, Kim, Lee, Cheong, Chung, et al., 2007). In particular, there is considerable interest in the use of physical methods to improve starch properties while maintaining food safety. Heat-moisture treatment (HMT) commonly occurs at a low moisture content (MC) (<35% H_2O, w/w) and at a temperature above the glass transition temperature (T_g) but below gelatinization temperature for a fixed period (15 min to 16 h). HMT has been reported as a green technique to alter the molecular, crystalline and granule structure and thus to regulate the granule swelling, amylose leaching, gelatinization parameters, viscosity, and enzyme susceptibility (Hoover,

2010; Jiranuntakul, Puttanlek, Rungsardthong, Puncha-arnon, & Uttapap, 2011; Zavareze & Dias, 2011). Generally, HMT-treated starches tended to have a higher gelatinization temperature, lower paste viscosity, decreased granule swelling degree, and increased thermal stability (Huang, Zhou, Jin, Xu, & Chen, 2015; Jacobs & Delcour, 1998; Jiranuntakul, et al., 2011). However, the change in enzyme susceptibility after HMT could depend on the starch source and treatment conditions (*e.g.*, temperature, moisture, and time) (Chung, Liu, & Hoover, 2009; Gunaratne & Hoover, 2002; Hoover, 2010; Kweon, Haynes, Slade, & Levine, 2000). Furthermore, while the digestibility of corn, potato and legume starches subjected by HMT has been extensively reported, few studies have been focused on the changes of digestibility of rice starch during HMT. Zavareze, Storck, de Castro, Schirmer, and Dias (2010) reported that the digestibility of rice starches with different amylose contents increased when HMT (110 °C and 1 h) was conducted with the moisture ranged from 15 to 25%. Besides, all of the above studies showed that the impact of HMT on starch digestibility depends on the HMT parameters, which can be linked to the changes of starch crystalline structure (crystallites disruption and changes in the polymorphic form) and morphology (formation of fissures and cracks on the granule surface).

The structure of starch is complex and considered to be organized on different length scales, comprised of the granule, the growth rings, and the semi-crystalline lamellae system (Pérez & Bertoft, 2010). This multi-scale packing of starch molecules has varying degrees of compactness, which with prominently different susceptibilities to enzyme hydrolysis (Zhang, Wang, Hasjim, Li, Flanagan, Gidley, et al., 2014). However, no systematic study has been undertaken to investigate the relationship between the starch multi-scale structure and the susceptibility of starch towards enzyme subjected to heat-moisture treatment (HMT). In particular, there is limited understanding of how the lamellar structure, helical structures, and short-range molecular orders regulate the starch digestion rate. Thus, from the view of the molecular level and molecular interactions, the mechanism regarding the structurally-modulated digestibility of rice starch was discussed. It is important to study the

relationships between the specific structures of starch as varied by HMT and its digestion rate, which is crucial for further understanding the health effects of resistant starch.

In this work, the effect of HMT on the granule morphology, semi-crystalline lamellae, crystallites, short-range molecular orders, helical conformations, and chain length and distribution of rice starch were investigated. Also, the related changes in the digestion rate were evaluated. In this way, the mechanism of the regulation of starch digestibility by HMT was revealed from the view of hierarchical structural changes. Moreover, the findings from the present study are crucial for the rational development of starch-based foods with tailored digestibility using HMT.

2. Materials and methods

2.1 Materials

The paddy rice was kindly supplied by South China Agricultural University. Standard amylose (A5012) and amylopectin (A8515) were obtained from Sigma-Aldrich (USA). Porcine pancreatic α-amylase (Cat. No.: P-7545, activity 8 × USP/g) and amyloglucosidase (A3306, > 300 u/mL) were purchased from Sigma-Aldrich (USA). The glucose oxidase-peroxidase assay kit (Cat. No.: K-GLUC) was obtained from Megazyme (Ireland).

2.2 Starch isolation

The paddy rice was soaked in distilled water at 4 °C for 24 h. The soaked rice grain was ground with a laboratory blender and passed through a 63μm sieve, followed by standing at 4 °C for 48 h. The supernatant solution was drained off, and the residue was diluted to the original volume with 0.4% sodium hydroxide solution, then stored at 4 °C for 48 h. The re-slurried starch was passed through a 63μm sieve again and kept at 4 °C for 24 h. The process was repeated three times, neutralized with 1M HCl to pH 7, washed with deionized water and dried overnight at 40 °C (Wang

& Wang, 2004). The moisture, protein and free lipid contents of rice starch were 10.32, 0.65 and 0.20 (g/100 g dry starch), respectively.

2.3 Heat-moisture treatment (HMT)

The HMT of rice starch was conducted under different moisture contents (*MC*) (10%, 20%, and 30%; coded as HMT-10, HMT-20, and HMT-30, respectively). The samples were equilibrated at 4 °C for 24 h. Then, they were placed in a 500mL screwed stainless steel reactor with continuous rotation and heated with oil at 110 °C for 4 h, followed by cooling to room temperature. During the HMT, the starch granules can be stirred by the paddle when the reactor was continuously rotated. In this way, the starch granules can be uniformly heated under a different *MC*. The treated samples were subsequently dried at 40 °C until the *MC* of the samples reached about 11% and then ground. The apparent amylose content (*AAC*) of starch samples were determined according to the method of Juliano, Perez, Blakeney, Castillo, Kongseree, Laignelet, et al. (1981).

2.4 In vitro digestibility

In-vitro starch digestibility was analyzed with a properly modified Englyst procedure (Englyst, Kingman, & Cummings, 1992). The enzyme solution was prepared as follows: 3 g of porcine pancreatic α-amylase was dispersed in 20 mL of deionized water with magnetical stirring and centrifuged at 3000 g for 25 min. The supernatant (13.5 mL) was transferred into a beaker and mixed with 0.7 mL of amyloglucosidase and 0.8 mL of deionized water. The enzyme solution was freshly prepared before use.

Starch (*ca.* 1 g) sample was placed into 100mL flasks. Acetate buffer (0.1 M, pH 5.2, 20 mL) was added using a pipette. Then, the flask was heated to boiling for 30 min. The boiled samples were cooled to 37 °C, and each was mixed with 5 mL of the enzyme solution, followed by incubation in a water bath at 37 °C with shaking (180 rpm). At different time intervals, 0.5 mL of hydrolysate was

collected, and 20 mL of 67% ethanol was added to deactivate the enzyme. The glucose concentration was calculated using the GOPOD assay. According to the rate of hydrolysis, starch was classified into rapidly-digestible starch (RDS, digested within 20 min), slowly-digestible starch (SDS, digested between 20 and 120 min), and resistant starch (RS, undigested within 120 min), respectively.

2.5 Structural characterization

2.5.1 Gel permeation chromatography (GPC) coupled with multi-angle light scattering (MALS)

The weight-average molecular molar mass (M_w) and molecular molar mass distribution of starch samples were analyzed using a GPC (Waters, USA) system equipped with a MALS detector (Wyatt, USA) and a refractive index detector. Three chromatographic columns (Styragel HR 3, Styragel HMW 6E, and Styragel HMW 7, Waters, USA) and a laser with a wavelength of 658 nm were used. Starch (*ca.* 5 mg) was dispersed in 10 mL of DMSO containing LiBr (50 mM) with heating in a boiling water bath for 1 h. The mobile phase was DMSO with LiBr (50 mmol/L) filtered through a 0.22 μm PTFE filter and degassed by ultrasound before use. Then, the sample was shaken at 60 °C for 12 h to ensure full dissolution of the starch in the mobile phase (Liu, Halley, & Gilbert, 2010). Before injection, the starch sample solutions were filtered using a 5μm membrane filter (Millipore Co., USA). The flow rate and total injected volume were 1.0 mL/min and 0.1 mL, respectively. The light scattering data were collected and analyzed using the Astra V software program.

2.5.2 Fourier transform Raman (FT-Raman) spectrometry

The FT-Raman spectra of starch samples were obtained by using a Nicolet iS50 instrument (ThermoFisher, USA) with a near-infrared YAG laser with a wavelength of 1064 nm. Spectra were recorded from the same spot size of each sample in the range of 4000 - 100 cm^{-1}, with a resolution of approximately 8 cm^{-1}. The full width at half height (*FWHH*) of the band at 480 cm^{-1} was used to

characterize the molecular order of starch. All measurements were performed at least five times to obtain the stable spectra.

2.5.3 ^{13}C CP/MAS Nuclear Magnetic Resonance (NMR) Spectroscopy

The solid-state ^{13}C CP/MAS NMR measurements were carried out at a ^{13}C frequency of 100.6 MHz on a Bruker Advance III HD 400 spectrometer (Bruker, Germany). About 200-300 mg of starch samples were packed in a 4-mm diameter, cylindrical, PSZ (partially stabilized zirconium oxide) rotor. ^{13}C spectra were recorded with at least 3000 scans, and the recycle delay was 2 s. The total spectra were deconvoluted into ordered and amorphous phases by subtracting a scaled amorphous starch spectrum until zero intensity was attained at 84 ppm for the difference spectrum (Tan, Flanagan, Halley, Whittaker, & Gidley, 2007).

2.5.4 X-ray diffraction (XRD)

The native and HMT-treated starches were equilibrated to a *MC* of about ~10% before the analysis. The crystalline structure of starch samples was evaluated using a powder X-ray diffractometer (PANalytical B.V., Netherlands), operating at 40 kV and 40 mA with Cu Kα radiation (λ) at 0.1542 nm. XRD patterns were acquired for a 2θ range from 4° to 40° with a step size of 0.033° and a step rate of 0.5 s per step. The relative crystallinity (*RC*) of each sample was calculated using the PeakFit software (Ver. 4.12).

2.5.5 Differential scanning calorimetry (DSC)

The thermal behaviors of samples were measured by a differential scanning calorimeter (DSC, PerkinElmer DSC 8000) with nitrogen purge gas. A high-pressure stainless steel pan (PerkinElmer No.B0182901) with a gold-plated copper seal (PerkinElmer NO.042e191758) was used for the measurements. About 3 mg of starch was accurately weighed and put into the DSC pan, followed by

the addition of distilled water (12 μL) was added with a microsyringe. An empty pan was used as a reference. The samples were scanned from 30 to 130 °C at a heating rate of 5 °C/min. The enthalpy change (ΔH), the onset temperature (T_o) and conclusion temperature (T_c) were calculated.

2.5.6 Synchrotron small-angle X-ray scattering (SAXS)

The lamellar characteristics of starch were investigated on the SAXS/WAXS beamline (flux, 1013 photons/s) at the Australian Synchrotron (Zhang, Chen, Xie, Li, Truss, Halley, et al., 2015) (Clayton, Vic, Australia), at a wavelength λ = 1.47 Å. The 2D scattering patterns were recorded through a Pilatus 1M camera (active area 169 × 179 mm; and pixel size 172 × 172 μm). Starch slurries with similar moisture levels (*ca.* 60%, w/w) were placed on a multi-well stage, and then the SAXS data were recorded for an acquisition time of 1 s. The scattering of pure water with Kapton tape (5413 AMBER 3/4IN X 36YD, 3M, USA) on the stage window was used as the background data. All the data were background subtracted and normalized. The data in the angular range of $0.0015 < q < 0.15$ Å^{-1} were used as the SAXS pattern, where $q = 4\pi\sin\theta/\lambda$, in which 2θ is the scattering angle and λ the X-ray wavelength.

SAXS curves were plotted as a function of the relative peak intensity I, versus q, the scattering vector. q is proportional to the inverse of the apparent periodic length d_{Bragg}, as $d_{Bragg} = 2\pi/q$ (Zhang, et al., 2015). Linear (*i.e.*, one-dimensional) correlation function was also used to analyze the corresponding parameters of the lamellar starch structure (Zhang, et al., 2015), as shown in Eq. (1):

$$f(r) = \frac{\int_0^\infty I(q)q^2 cos(qr)dq}{\int_0^\infty I(q)q^2 dq} \quad (1)$$

In this equation, r (nm) is the distance in the real space, and d is the second maximum of $f(r)$ (lamellar repeat distance, *i.e.*, the thickness of semi-crystalline lamellae). d_a, representing amorphous lamellae thickness of the semi-crystalline structure, can be acquired by the solution of the linear region and the flat $f(r)$ minimum. Therefore, d_c, the crystalline lamellae thickness of the semi-crystalline structure, is calculated by $d_c = d - d_a$.

2.5.7 Scanning electron microscopy (SEM)

A starch sample was spread on an SEM stub with double-sided adhesive tape and coated with gold. Scanning electron micrographs were taken using a scanning electron microscope (EVO18, ZEISS, Germany) operated at 10.0 kV high voltages.

2.5.8 Particle size measurements of starch granules

A Mastersizer 2000 laser diffraction particle size analyzer (Version 5.22, Malvern, England) was used to detect the starch particle size parameters, *i.e.*, specific surface area (*SpSA*) and mean particle size (D_{50}). Each sample was added to the reservoir and fully dispersed in anhydrous ethanol until an obscuration value between 12% and 17% was achieved. The optical mode was Mie with a refractive index (*RI*) of starch and the dispersing reagent ethanol of 1.54 and 1.36, respectively.

2.6 Statistical Analysis

All the experiments were performed at least in triplicate, and experimental data were analyzed using analysis of variance (ANOVA) and expressed as mean value ± standard deviation. The significant differences were determined using Tukey's HSD test ($P < 0.05$) with the SPSS 22.0 statistical software for Windows (SPSS, Inc., Chicago, IL).

3. Results and discussion

3.1 In vitro digestibility

Table 1 shows the digestibility data of native and HMT starches. As expected, compared to native rice starch, HMT starches had less content of RDS, but more contents of SDS and RS, indicating that HMT could reduce the starch digestion rate by transforming some fractions of RDS into SDS and RS. In particular, the increases in SDS and RS portions were more evident with higher

MC, suggesting that *MC* played a major role in controlling the digestibility of HMT samples, which is in agreement with the case of mung bean starch (Li, Ward, & Gao, 2011). In particular, the treated rice starch with 30% *MC* showed a high SDS + RS content (25.0%), which had extensive increase compared with other starches (Ambigaipalan, Hoover, Donner, & Liu, 2014; Huang, et al., 2015; Li, et al., 2011). Furthermore, after HMT, the *AAC* gradually increased with higher *MC*. Regarding this, HMT could favor the formation of the complexes within the grain reducing the quantification of amylose by the method used.

3.2 Molecular molar mass and its distribution

As shown in **Table 1**, the weight-average molecular molar mass (M_w) of native and HMT starches. With higher *MC*, M_w of HMT starches was gradually decreased to 6.228×10^6 g/mol. Meanwhile, the mean square radius of gyration (R_g) was decreased with lower M_w. The changes in M_w and R_g indicated the degradation of starch molecules resulting from HMT.

For further understanding the characteristic of starch molecules subjected to HMT, the cumulative weight fractions at different M_w ranges were investigated. Specifically, the range of M_w of native starch was higher, and the fractions in the ranges of 1×10^7-3×10^7 g/mol and > 3×10^7 g/mol accounted for 41.44% and 58.56%, respectively. After HMT, the molecular distribution of starch moved towards lower M_w. At 30% *MC*, M_w was in the range of 2×10^6-5×10^6 g/mol. Our group has reported that the maize starch molecules with M_w between 4×10^5 to 4×10^6 g/mol could preferably form RS and the starch molecules with M_w below 4×10^4 g/mol could be easily digested by the enzyme (Pu, Chen, Li, & Li, 2013).

3.3 Short-range ordered molecular structure

Raman spectra can be used to characterize the degree of short-range ordered structure in starch. The FT-Raman spectra of native and HMT rice starches are shown in **Fig. 1**. Several clear

characteristic bands could be seen at 480, 865, 943, 1264 and 2900 cm^{-1}, which are related to δ (CH_2), υ_s (C1-O-C4), υ_s (C1-O-C5), skeletal (C-C-O), and υ (C-H) modes, respectively (Mutungi, Passauer, Onyango, Jaros, & Rohm, 2012). Among these bands, the full width at half height (*FWHH*) of the band at 480 cm^{-1} is often used to characterize the short-range ordered molecular structure of starch. The higher the *FWHH* of the band at 480 cm^{-1}, the lower is the degree of molecular ordering of starch (Flores-Morales, Jiménez-Estrada, & Mora-Escobedo, 2012). The *FWHH* values (see **Table 2**) for rice starches after HMT were higher than those of their native counterpart, indicating that the short-range ordered molecular structure of rice starch was decreased after HMT.

3.4 Helical conformations

To further identify the changes of different short-range ordered molecular structure (the single- and double-helical structures) of rice starch after HMT, the solid-state ^{13}C CP/MAS NMR spectra of native and HMT rice starches were obtained (see **Fig. S1**)**.** After HMT, the shapes of peaks corresponding to the starch carbons C1 and C2,3,5 showed a notable change, while the peaks associated with C4 and C6 was not apparently altered. The peaks at around 102 and 103 ppm in the C1 region are typical characteristics of V-type single helices (eight glucose cycles per turn), and 103 ppm is also related to the amorphous starch associated with the junction points of amylopectin double helices (Fan, Ma, Wang, Huang, Zhang, Zhao, et al., 2013; Mihhalevski, Heinmaa, Traksmaa, Pehk, Mere, & Paalme, 2012). Furthermore, the peaks at *ca.* 101.5, 100.5 and 99.4 ppm (data not shown) in the C1 region indicates that the double-helical structures in the starch are A-type double helices. These peaks were used to study the changes in the short-range double helices.

To evaluate the relative proportions of different helical structure of native and HMT starches, the solid-state ^{13}C CP/MAS NMR spectra were deconvoluted into amorphous and ordered sub-spectra, using intensity at 84 ppm as a reference. The detailed alterations to the amorphous and

helical conformations are shown in **Table 2**. The double helix fractions of HMT starches were gradually reduced with the increased *MC*, indicating that HMT disrupted the intermolecular hydrogen bonding. Also, the percentage of amorphous starch was reduced. However, with the increased *MC* during HMT, the content of single helices (*i.e.*, V-type) was increased, suggesting that HMT facilitated the formation of V-type single-helical conformation. However, the percentage of V-type crystalline structure reached a plateau value between 10 and 20% *MC*, which might be related to the amount of lipids available for the V-type amylose complexes.

3.5 Crystalline structure

Fig. 2 shows the XRD patterns of rice starch before and after HMT. Native rice starch showed an A-type polymorph. After HMT, rice starch did not show any changes in the type of crystalline structure except a slight reduction in the diffraction peak intensities. However, an apparent increase in peak intensity at 20° (Vamadevan, Hoover, Bertoft, & Seetharaman, 2014) appeared at a high *MC* (especially at 30% *MC*), indicating the formation of amylose-lipid (black arrows) complex during HMT. The X-ray intensities of the strongest peaks at 20° increased by 1.4 and 1.7 times for HMT-20 and HMT-30, respectively, compared to native rice starch. Previous studies have reported that amylose-lipid complexes form a significant fraction in improving the enzymatic resistance (Guraya, Kadan, & Champagne, 1997; Hasjim, Lee, Hendrich, Setiawan, Ai, & Jane, 2010).

Table 2 shows that HMT decreased the *RC* of rice starch, especially with higher *MC*. This result was as expected as during HMT, water could promote the disruption of intra- and intermolecular hydrogen bonding in starch granules (Hoover, 2010), resulting in a decreased regularity of the molecular packing.

3.6 Ordered molecular structure

The thermal transition parameters are summarized in **Table 2**. One endotherm (G) was observed for native starch, while there were two endotherms (G and M) for HMT starches (see in **Fig. S2**). The G and M endotherms are respectively attributed to the melting of ordered amylopectin side chains (crystallites and double-helices), and amylose-lipid complexes and/or the complexes formed by degraded short linear starch chains (Zhang, Zhao, Li, Li, Xie, & Chen, 2014). The transition enthalpy ΔH was positively correlated to the amount of long- and short-range starch ordered structures. After HMT, rice starch showed a prominent reduction in ΔH, especially at 30% *MC*, indicating that some part of starch ordered structures with flaws were disorganized by HMT. However, with elevated *MC* during HMT, the onset (T_o) and conclusion (T_c) temperatures of G endotherm were increased. The higher T_o and T_c values indicated the formation of the ordered starch molecular structures (amylopectin crystallites and double-helices) with higher thermal stability. Regarding the M endotherm, the formation of new complexes suggested the greater flexibility and mobility of starch chains for re-arrangement during HMT, especially at higher *MC*, which also had higher heat resistance.

3.7 Lamellar structural characteristics

Fig. 3 shows the SAXS patterns (log-log) of native and HMT starches. All starch samples displayed a scattering peak at *ca.* 0.06 $Å^{-1}$, corresponding to the periodic length (d_{Bragg}) of semi-crystalline lamellae of starch with the Woolf-Bragg's equation $d_{Bragg}=2\pi/q$. To further investigate the alterations of semi-crystalline lamellae, the average thicknesses of semi-crystalline (d), crystalline (d_c) and amorphous (d_a) lamellae were also obtained using Eq. (1). The lamellar parameters are recorded in **Table 2**. The difference between d and d_{Bragg} was seen since d_{Bragg} obtained by the Woolf-Bragg approach is always greater than d. After HMT, slight increases in the thicknesses of semi-crystalline (d), crystalline (d_c) and amorphous (d_a) lamellae were observed as the *MC* rose (especially at 30%). These results suggested that HMT could simultaneously increase both the

thicknesses of amorphous (d_a) and crystalline (d_c) lamellae of rice starch. The increase in d_a might mainly result from the swelling in amorphous lamellae or the disassociation of some tailing ends of double helices. In other words, the amorphous parts were less tightly packed after HMT. Regarding the increase in d_c, it was speculated that water and thermal energy induced the packing of some tailing ends of double helices or the partial breakage of the hydrogen bonds of starch molecular helices in the starch granule interior, which led to a irregular rearrangement of double helices in crystalline lamellae.

The difference in electron density within the aggregation structure could lead to different scattering intensity (Qiao, Yu, Liu, Zou, Xie, Simon, et al., 2016). The lamellae with a high degree of order contributed to the SAXS peak with fine visibility and an apparent peak at *ca.* 0.06 $Å^{-1}$. From **Table 2**, it is seen that HMT reduced the intensity and area of the peak, indicating a reduced ordering degree of semi-crystalline lamellae. This decrease was presumably due to the molecular-helical dissociation, the disordering of the crystalline structure, and the irregular re-arrangement.

3.8 Morphology and size distribution of starch

Fig. 4 shows the morphology of native and HMT starch granules. The native granules were small and had angular, polyhedral shapes with smooth surfaces. HMT with 10% *MC* did not affect the morphology of rice starch granules. However, HMT at 20% and 30% *MC* evidently affected the form and degree of agglomeration of the granules. In these cases, there was a higher degree of agglomeration of granules, and the granule surface became slightly rougher, as compared with native and HMT-10 starches. This observation was reasonable as the moisture and thermal energy during HMT could result in partial gelatinization leading to the inconsistent swelling of the granules and the appearance of concavities on the surfaces, particularly at a high *MC* (*i.e.*, 30%), which was in agreement with earlier reports (Zavareze, et al., 2010).

The evolutions of granule volume size distributions of rice starch before and after HMT are summarized in **Table 1**. After HMT, rice starch granules presented an increase in their granule size, as shown by a shift of the size distribution profile and the mean particle size towards a larger particle size range (see in **Fig. S3**). With the increased *MC*, a gradual increase in the particle size was seen for rice starch granules. Regarding this result, it was possible that HMT induced the occurrence of re-aggregation (agglomeration) of small granules, which was in agreement with SEM results. Furthermore, specific surface area (*SpSA*) of starch granules was gradually declined by HMT with increased *MC*. Moreover, the larger particle size and lower *SpSA* could impede the diffusion and adsorption of enzymes, leading slower digestion of starches (de la Hera, Gomez, & Rosell, 2013).

3.9 Mechanism of structure changes and enzymatic resistivity after HMT

HMT can induce a greater flexibility and mobility of starch chains, leading to the disruption of intra- and intermolecular hydrogen bonds in starch granules (Ambigaipalan, et al., 2014). The rupture of hydrogen bonds resulted in the dissociation of double helices and the unraveling of helices, followed by the distortion (irregular re-arrangement and packing) of the lattice, eventually disrupted the crystalline structure of rice starches. With the increased *MC*, the supramolecular structure was more significantly disorganized. Regarding this, increasing the *MC* would increase the molecular motion, eventually led to greater mobility of the semi-crystalline lamellae. Furthermore, the increased *MC* during HMT gradually degraded the starch chains. Therefore, the molecular fragments with low M_w ($< 1\times10^7$ g/mol) gradually were increased, especially at 30% *MC*.

Due to the greater degree of the molecular mobility, the structural re-assembly on multiple lengths scales simultaneously occurred during the HMT, accompanying the structural disordering and degradation. The motion of starch chains allowed the formation of new aggregation structures, as shown by the increased amounts of single-helices (a highly-ordered starch matrix) and densely-packed amorphous starch molecules. Besides, the disassociation and re-arrangement of starch

molecular helices led to the increased thicknesses of crystalline and amorphous lamellae. Again, despite the reduced amorphous content, the amorphous parts became less tightly packed resulting from HMT.

By inspecting the SDS + RS contents and the structural characteristics of the samples after HMT at 20% and 30% *MC*, it was proposed that SDS and RS were preferably formed by the degraded starch molecules with M_w between 4×10^5 to 4×10^6 g/mol, single helices, amylose-lipids complexes with higher thermal stability, and crystalline lamellae of higher thickness. In other words, HMT induced the changes of starch multi-scale structures, with the formation of a new ordered molecular aggregation architecture that was more resistant to the enzyme attack. These structural changes accounted for the higher content of resistant starch.

4. Conclusion

The changes in *vitro* digestibility and the multi-scale structure of rice starch during HMT have been investigated. Depending on the *MC* during HMT, the structures on different length scales were changed to different degrees, along with starch digestibility. With HMT, semi-crystalline lamellae, crystalline structure, short-range ordered structures, and double helical conformation could be modified, together with the degradation of starch molecules. The re-arrangement of starch granules and starch molecules occurred, which facilitated the formation of agglomerated starch granules, and aggregated starch molecules with a higher degree of ordering. This re-arrangement, accompanying the disorganization of the original orders, transformed part of RDS into SDS and RS, eventually resulted in a significant increase in SDS and RS contents. The results from present work are valuable to design starch products with tailored digestion behavior through controlling the changes of starch multi-scale structure.

Conflict of interest

The authors declare no conflicts of interest.

Acknowledgments

This work is supported by the Key Project of the National Natural Science Foundation of China (NSFC)-Guangdong Joint Foundation Key Project (U1501214), the National Key Research and Development Programa of China (2016YFD04012021), YangFan Innovative and Entrepreneurial Research Team Project (No. 2014YT02S029), the Key R&D Projects of Zhongshan (2014A2FC217), the R&D Projects of Guangdong Province (2014B090904047), NSFC (31271824), the Science and Technology Program of Guangzhou (201607010109), the Innovative Projects for Universities in Guangdong Province (2015KTSCX006), and the Fundamental Research Funds for the Central Universities (2015ZZ106). Part of this research was undertaken on the SAXS/WAXS beamline at the Australian Synchrotron, Victoria, Australia.

Appendix A. Supplementary data

Supplementary data associated with this article can be found in Appendix A.

References

Ambigaipalan, P., Hoover, R., Donner, E., & Liu, Q. (2014). Starch chain interactions within the amorphous and crystalline domains of pulse starches during heat-moisture treatment at different temperatures and their impact on physicochemical properties. *Food Chemistry, 143*, 175-184.

Chung, H.-J., Liu, Q., & Hoover, R. (2009). Impact of annealing and heat-moisture treatment on rapidly digestible, slowly digestible and resistant starch levels in native and gelatinized corn, pea and lentil starches. *Carbohydrate Polymers, 75*(3), 436-447.

de la Hera, E., Gomez, M., & Rosell, C. M. (2013). Particle size distribution of rice flour affecting the starch enzymatic hydrolysis and hydration properties. *Carbohydrate Polymers, 98*(1), 421-427.

Edes, T. E., & Shah, J. H. (1998). Glycemic index and insulin response to a liquid nutritional formula compared with a standard meal. *Journal of the American College of Nutrition, 17*(1), 30-35.

Englyst, H. N., Kingman, S. M., & Cummings, J. H. (1992). Classification and measurement of nutritionally important starch fractions. *European Journal of Clinical Nutrition, 46 Suppl 2*, S33-50.

Englyst, K. N., Vinoy, S., Englyst, H. N., & Lang, V. (2007). Glycaemic index of cereal products explained by their content of rapidly and slowly available glucose. *British Journal of Nutrition, 89*(3), 329-339.

Fan, D., Ma, W., Wang, L., Huang, J., Zhang, F., Zhao, J., Zhang, H., & Chen, W. (2013). Determining the effects of microwave heating on the ordered structures of rice starch by NMR. *Carbohydrate Polymers, 92*(2), 1395-1401.

Flores-Morales, A., Jiménez-Estrada, M., & Mora-Escobedo, R. (2012). Determination of the structural changes by FT-IR, Raman, and CP/MAS ^{13}C NMR spectroscopy on retrograded starch of maize tortillas. *Carbohydrate Polymers, 87*(1), 61-68.

Gunaratne, A., & Hoover, R. (2002). Effect of heat–moisture treatment on the structure and physicochemical properties of tuber and root starches. *Carbohydrate Polymers, 49*(4), 425-437.

Guraya, H. S., Kadan, R. S., & Champagne, E. T. (1997). Effect of rice starch-lipid complexes on in vitro digestibility, complexing index, and viscosity. *Cereal Chemistry Journal, 74*(5), 561-565.

Hasjim, J., Lee, S.-O., Hendrich, S., Setiawan, S., Ai, Y., & Jane, J.-l. (2010). Characterization of a novel resistant-starch and its effects on postprandial plasma-glucose and insulin responses. *Cereal Chemistry Journal, 87*(4), 257-262.

Hoover, R. (2010). The impact of heat-moisture treatment on molecular structures and properties of starches isolated from different botanical sources. *Critical Reviews in Food Science and Nutrition, 50*(9), 835-847.

Hu, P., Zhao, H., Duan, Z., Linlin, Z., & Wu, D. (2004). Starch digestibility and the estimated glycemic score of different types of rice differing in amylose contents. *Journal of Cereal Science, 40*(3), 231-237.

Huang, T.-T., Zhou, D.-N., Jin, Z.-Y., Xu, X.-M., & Chen, H.-Q. (2015). Effect of debranching and heat-moisture treatments on structural characteristics and digestibility of sweet potato starch. *Food Chemistry, 187*, 218-224.

Jacobs, H., & Delcour, J. A. (1998). Hydrothermal modifications of granular starch, with retention of the granular structure: A review. *Journal of Agricultural and Food Chemistry, 46*(8), 2895-2905.

Jiranuntakul, W., Puttanlek, C., Rungsardthong, V., Puncha-arnon, S., & Uttapap, D. (2011). Microstructural and physicochemical properties of heat-moisture treated waxy and normal starches. *Journal of Food Engineering, 104*(2), 246-258.

Juliano, B. O., Perez, C. M., Blakeney, A. B., Castillo, T., Kongseree, N., Laignelet, B., Lapis, E. T., Murty, V. V. S., Paule, C. M., & Webb, B. D. (1981). International cooperative testing on the amylose content of milled rice. *Starch - Stärke, 33*(5), 157-162.

Kweon, M., Haynes, L., Slade, L., & Levine, H. (2000). The effect of heat and moisture treatments on enzyme digestibility of *AeWx*, *Aewx* and *aeWx* corn starches. *Journal of Thermal Analysis and Calorimetry, 59*(1), 571-586.

Lee, C. J., & Moon, T. W. (2015). Structural characteristics of slowly digestible starch and resistant starch isolated from heat–moisture treated waxy potato starch. *Carbohydrate Polymers, 125*, 200-205.

Li, S., Ward, R., & Gao, Q. (2011). Effect of heat-moisture treatment on the formation and physicochemical properties of resistant starch from mung bean (*Phaseolus radiatus*) starch. *Food Hydrocolloids, 25*(7), 1702-1709.

Liu, W.-C., Halley, P. J., & Gilbert, R. G. (2010). Mechanism of degradation of starch, a highly branched polymer, during extrusion. *Macromolecules, 43*(6), 2855-2864.

Miao, M., Zhang, T., Mu, W., & Jiang, B. (2010). Effect of controlled gelatinization in excess water on digestibility of waxy maize starch. *Food Chemistry, 119*(1), 41-48.

Mihhalevski, A., Heinmaa, I., Traksmaa, R., Pehk, T., Mere, A., & Paalme, T. (2012). Structural changes of starch during baking and staling of rye bread. *Journal of Agricultural and Food Chemistry, 60*(34), 8492-8500.

Mutungi, C., Passauer, L., Onyango, C., Jaros, D., & Rohm, H. (2012). Debranched cassava starch crystallinity determination by Raman spectroscopy: Correlation of features in Raman spectra with X-ray diffraction and ^{13}C CP/MAS NMR spectroscopy. *Carbohydrate Polymers, 87*(1), 598-606.

Pérez, S., & Bertoft, E. (2010). The molecular structures of starch components and their contribution to the architecture of starch granules: A comprehensive review. *Starch - Stärke, 62*(8), 389-420.

Pu, H., Chen, L., Li, L., & Li, X. (2013). Multi-scale structural and digestion resistibility changes of high-amylose corn starch after hydrothermal-pressure treatment at different gelatinizing temperatures. *Food Research International, 53*(1), 456-463.

Qiao, D., Yu, L., Liu, H., Zou, W., Xie, F., Simon, G., Petinakis, E., Shen, Z., & Chen, L. (2016). Insights into the hierarchical structure and digestion rate of alkali-modulated starches with different amylose contents. *Carbohydrate Polymers, 144*, 271-281.

Shin, S. I., Lee, C. J., Kim, D.-I., Lee, H. A., Cheong, J.-J., Chung, K. M., Baik, M.-Y., Park, C. S., Kim, C. H., & Moon, T. W. (2007). Formation, characterization, and glucose response in mice to rice starch with low digestibility produced by citric acid treatment. *Journal of Cereal Science, 45*(1), 24-33.

Shu, X., Jia, L., Ye, H., Li, C., & Wu, D. (2009). Slow digestion properties of rice different in resistant starch. *Journal of Agricultural and Food Chemistry, 57*(16), 7552-7559.

Tan, I., Flanagan, B. M., Halley, P. J., Whittaker, A. K., & Gidley, M. J. (2007). A method for estimating the nature and relative proportions of amorphous, single, and double-helical components in starch granules by ^{13}C CP/MAS NMR. *Biomacromolecules, 8*(3), 885-891.

Vamadevan, V., Hoover, R., Bertoft, E., & Seetharaman, K. (2014). Hydrothermal treatment and iodine binding provide insights into the organization of glucan chains within the semi-crystalline lamellae of corn starch granules. *Biopolymers, 101*(8), 871-885.

Wang, L., & Wang, Y.-J. (2004). Rice starch isolation by neutral protease and high-intensity ultrasound. *Journal of Cereal Science, 39*(2), 291-296.

Yang, C. Z., Shu, X. L., Zhang, L. L., Wang, X. Y., Zhao, H. J., Ma, C. X., & Wu, D. X. (2006). Starch properties of mutant rice high in resistant starch. *Journal of Agricultural and Food Chemistry, 54*(2), 523-528.

Zavareze, E. d. R., & Dias, A. R. G. (2011). Impact of heat-moisture treatment and annealing in starches: A review. *Carbohydrate Polymers, 83*(2), 317-328.

Zavareze, E. d. R., Storck, C. R., de Castro, L. A. S., Schirmer, M. A., & Dias, A. R. G. (2010). Effect of heat-moisture treatment on rice starch of varying amylose content. *Food Chemistry, 121*(2), 358-365.

Zhang, B., Chen, L., Xie, F., Li, X., Truss, R. W., Halley, P. J., Shamshina, J. L., Rogers, R. D., & McNally, T. (2015). Understanding the structural disorganization of starch in water-ionic liquid solutions. *Physical Chemistry Chemical Physics, 17*(21), 13860-13871.

Zhang, B., Wang, K., Hasjim, J., Li, E., Flanagan, B. M., Gidley, M. J., & Dhital, S. (2014). Freeze-drying changes the structure and digestibility of B-polymorphic starches. *Journal of Agricultural and Food Chemistry, 62*(7), 1482-1491.

Zhang, B., Zhao, Y., Li, X., Li, L., Xie, F., & Chen, L. (2014). Supramolecular structural changes of waxy and high-amylose cornstarches heated in abundant water. *Food Hydrocolloids, 35*, 700-709.

Zhang, T., Li, X., Chen, L., & Situ, W. (2016). Digestibility and structural changes of waxy rice starch during the fermentation process for waxy rice vinasse. *Food Hydrocolloids, 57*, 38-45.

Zhou, Z., Robards, K., Helliwell, S., & Blanchard, C. (2002). Composition and functional properties of rice. *International Journal of Food Science & Technology, 37*(8), 849-868.

Figure Captions

Fig. 1. Raman spectra of native and HMT rice starches (10, 20 or 30 represents the HMT moisture content, %).

Fig. 2. X-ray diffraction patterns of native and HMT rice starches (10, 20 or 30 represents the HMT moisture content, %).

Fig. 3. Double logarithmic SAXS patterns of native and HMT rice starches (10, 20 or 30 represents the HMT moisture content, %).

Fig. 4. SEM images of native and HMT rice starch granules (magnification: 5000×; 10, 20 or 30 represents the HMT moisture content, %).

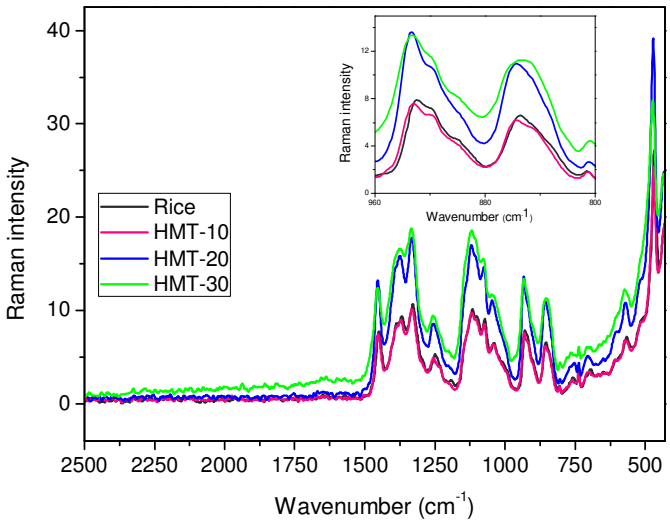

Fig. 1

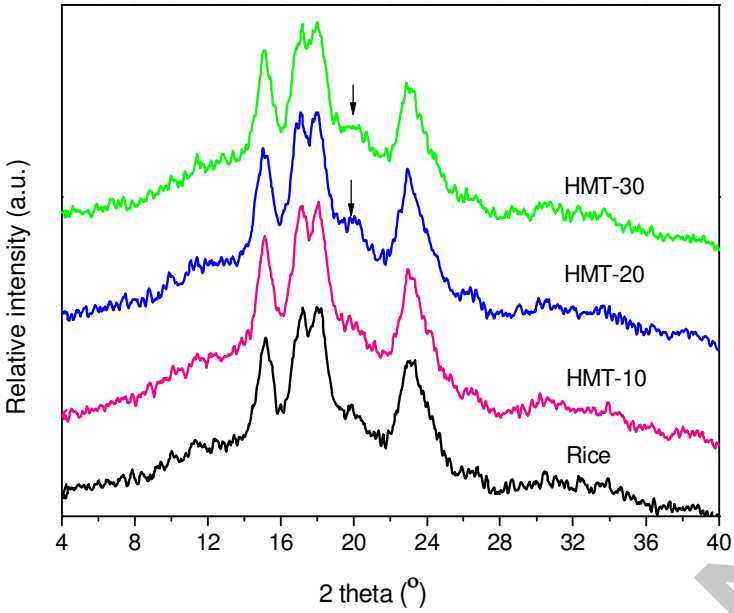

Fig. 2

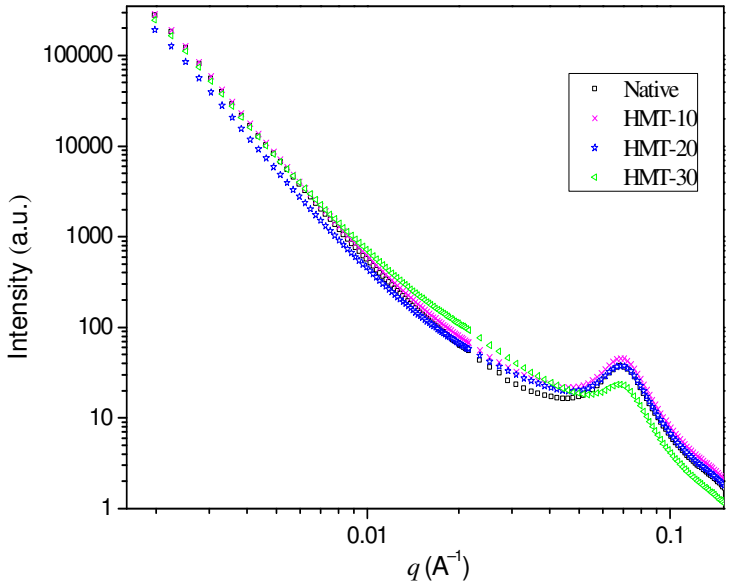

Fig. 3

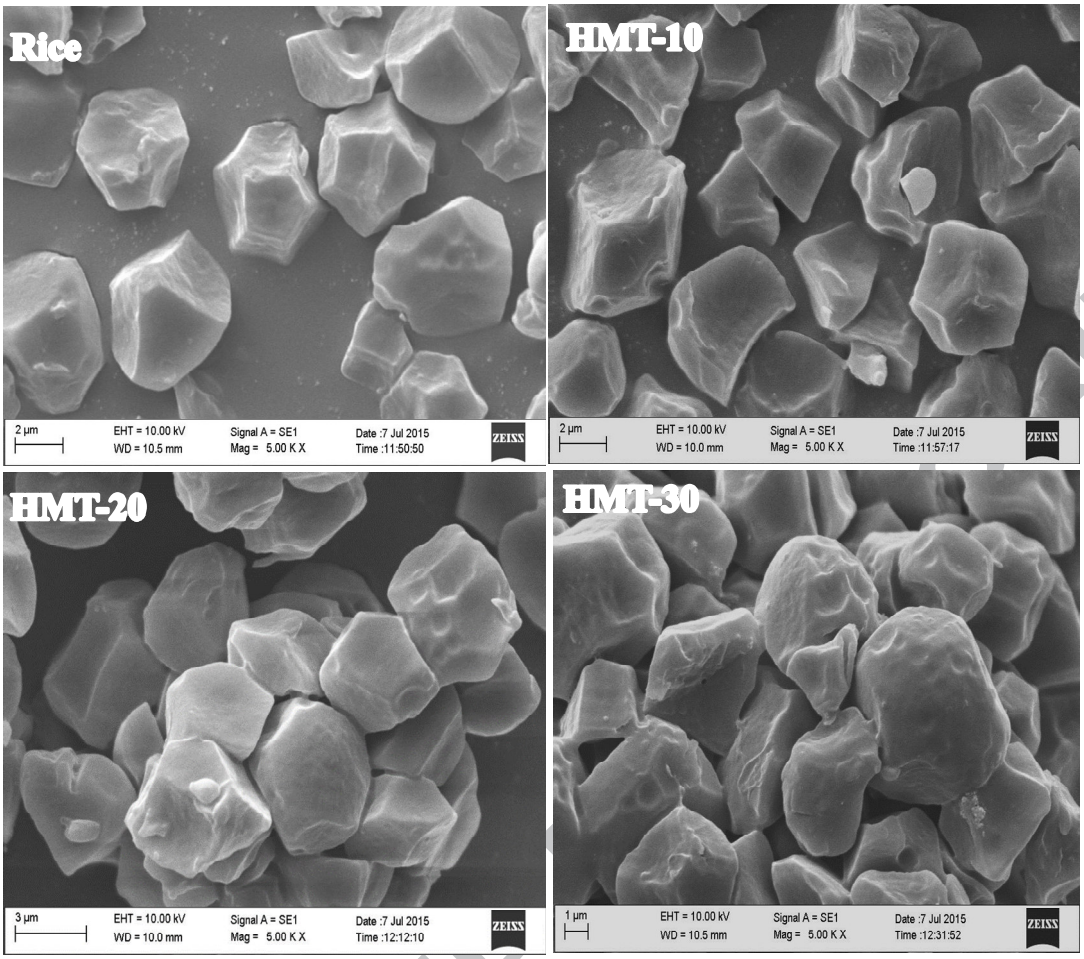

Fig. 4

Table 1. Digestibility, apparent amylose contents, granule sizes, and molar mass distribution of native and HMT rice starches (10, 20 or 30 represents the HMT moisture content, %)[A]

		Native starch	HMT-10	HMT-20	HMT-30
RDS (%)		93.9±1.5^{a}	84.0±2.1^{b}	75.2±2.3^{c}	75.0±2.1^{c}
SDS (%)		3.5±0.8^{c}	8.3±0.7^{b}	11.0±0.7^{a}	10.5±1.6^{a}
RS (%)		2.6±0.5^{d}	7.7±0.8^{c}	13.8±1.0^{b}	14.5±1.9^{b}
AAC (%)		13.5±0.1^{c}	14.1±0.3^{b}	14.7±0.2^{b}	15.4±0.3^{a}
D_{50} (μm)		6.25±1.13^{d}	9.81±1.45^{c}	61.98±2.19^{b}	177.3±5.64^{a}
SpSA (m^2/g)		1.30±0.15^{a}	0.57±0.03^{b}	0.12±0.02^{c}	0.08±0.00^{d}
M_w (g/mol)		4.131×10^7 (2%)	2.009×10^7 (1%)	1.840×10^7 (2%)	6.228×10^6 (1%)
R_g (nm)		127.0 (2.0%)	124.5 (1.0%)	109.8 (1.0%)	118.9 (1.0%)
Molar mass distribution (%)	2×10^6–5×10^6 g/mol	0	0	25.95	58.34
	5×10^6–1×10^7 g/mol	0	21.99	24.05	19.92
	1×10^7–3×10^7 g/mol	41.44	53.01	39.51	21.74
	>3×10^7 g/mol	58.56	25.00	10.49	0

[A] Means followed by different letters in the same line are significantly different at $P < 0.05$.

Table 2. XRD, Raman spectroscopy, SAXS, DSC and NMR parameters of native and HMT rice starches (10, 20 or 30 represents the HMT moisture content, %)[A]

		Native starch	HMT-10	HMT-20	HMT-30
	RC (%)	31.9±2.8^a	29.7±1.9^b	29.2±2.1^b	26.3±1.4^c
	FWHH	17.2±0.4^c	17.4±0.1^c	20.2±0.2^b	23.2±0.2^a
	Peak Area	10.30±0.01^a	10.23±0.02^a	9.92±0.02^b	7.75±0.01^c
	d_{Bragg} (nm)	9.17±0.01^b	9.17±0.02^b	9.20±0.00^b	9.24±0.01^a
	d (nm)	8.98±0.02^c	8.98±0.01^c	9.01±0.01^b	9.14±0.02^a
	d_a (nm)	2.82±0.01^b	2.82±0.00^b	2.82±0.01^b	2.87±0.02^a
	d_c (nm)	6.16±0.00^c	6.16±0.01^c	6.19±0.00^b	6.27±0.01^a
	T_o (°C)	60.00±0.32^d	61.35±0.25^c	64.54±0.21^b	66.11±0.36^a
G	T_c (°C)	77.47±0.43^d	82.52±0.23^c	88.07±0.31^a	83.69±0.26^b
	Δ*H* (J/g)	15.98±0.45^a	15.53±0.55^a	13.40±0.52^b	10.45±0.37^d
	T_o (°C)	–	–	98.81±0.21^b	111.8±0.26^a
M2	T_c (°C)	–	–	112.8±0.23^b	120.0±0.32^a
	Δ*H* (J/g)	–	–	0.89±0.23^a	0.88±0.19^a
	Double helix (%)	38.6±1.5^a	36.0±1.7^b	34.3±1.2^c	30.4±2.0^d
	Single helix (%)	4.2±0.9^c	5.4±1.1^b	12.1±1.2^a	12.8±0.2^a
	Amorphous (%)	57.2±2.3^b	58.6±2.5^a	53.6±1.7^d	56.8±2.6^c

[A]Means followed by different letters in the same line are significantly different at $P < 0.05$.

Highlights

- ✓ HMT transformed part of RDS into SDS and RS for rice starch
- ✓ HMT induced concomitant structural disorganization and molecular rearrangement
- ✓ Higher moisture content led to greater change in starch digestibility and structure
- ✓ More ordered structure and greater d_c thickness led to higher enzymatic resistance